JTTEE5 18:652–664
DOI: 10.1007/s11666-009-9397-z
1059-9630/$19.00 © ASM International

Peer Reviewed

Wear Resistance Improvement of Small Dimension Invar Massive Molds for CFRP Components

C. Giolli, M. Turbil, G. Rizzi, M. Rosso, and A. Scrivani

(Submitted February 28, 2009; in revised form August 5, 2009)

Invar alloy (Fe-36%Ni) is used in industrial applications that require high dimensional stability because of its exceptionally low thermal expansion coefficient. The purpose of this work is to improve the wear resistance of the molds in the production of carbon-fiber reinforced plastic (CFRP) components applying thermal spray coatings. Four different kinds of commercial powders were coated on an Invar substrate: ZrO_2-8Y_2O_3, Al_2O_3-13TiO_2, and Cr_2O_3 by air plasma spray (APS) and WC-CoCr by high-velocity oxygen fuel (HVOF). Metallographic microscopy observation and scanning electron microscopic analysis were carried out, microhardness and fracture toughness were evaluated using the microindentation method. Friction behavior and wear resistance were evaluated with pin-on-disk apparatus. Tungsten carbide coating had the lowest average coefficient of friction. Cermet and alumina-titania coatings showed the lowest wear mass loss. Among the APS ceramic coatings, alumina-titania exhibited the best wear behavior and the HVOF cermet coating exhibited the best behavior among all the coatings.

Keywords APS coatings, cermet coatings, friction and wear, INVAR tooling, properties

1. Introduction

One of the most important tasks of composite manufacturing is its capability to produce components that require a precise and specified shape within tight dimensional tolerances. The first step of this composite-forming procedure is the cut and layup of several prepreg layers on a mold surface with varying orientation in order to produce a laminate of the desired thickness. The assembly is then covered with a flexible vacuum bag and cured in autoclave, in which heat and pressure are simultaneously applied; the selection of a proper cure cycle is a key factor in producing a high-quality composite part and for ensuring high production rates. A typical autoclave cure cycle consists of a two-hold cycle in which the temperature of the autoclave is first raised from room temperature to 135 °C at a ramp rate of 5 °C/min and held for 160 min, and then raised to 177 °C (typical curing temperature of the carbon fiber/epoxy resins) at a ramp rate of 1 °C/min and hold for 120 min. During this process, the autoclave pressure is maintained at a constant 4.8×10^5 Pa. Before taking out the mold from the autoclave and removing the composite part from the mold, both the autoclave and the part are left to cool down slowly to room temperature (Ref 1, 2). However, the greatest difficulty comes during the autoclave processing of composite structures as residual stresses can cause shape dimensional changes, that is, a curvature in the middle of initially flat parts (*warpage*) and a reduction of enclosed angles in parts with a curved geometry (*spring-in*). Several parameters have been identified as possible causes of this residual stress buildup during autoclave cure cycles, and these are classified in intrinsic parameters (related to part geometry and material properties) such as a differential thermal expansion between fibers and matrix, layup orientation and part thickness and shape, and extrinsic parameters (related to tooling and processing) as heating up and cooling down rates and autoclave pressure during cure of composite parts (Ref 3, 4).

It was observed that mold material plays a critical role in warpage and spring-in generation. The explanation of this behavior is often attributed to a mismatch between the coefficient of thermal expansion (CTE) of the mold material and the one of the composite material that is to be cured. When the autoclave pressure is applied and the temperature increases, molds with considerably higher CTE expand thermally, applying a shear stress to the composite layers. In the early stages of the process, when the resin is not cured, slippage of the layers between one and another occurs, leading to a stress release in layers furthest from the mold surface. This creates through the thickness of the laminate a stress gradient, decreasing in

This article is an invited paper selected from presentations at the 2008 International Thermal Spray Conference and has been expanded from the original presentation, which was published in *Thermal Spray 2008: Thermal Spray Crossing Borders*, on CD-ROM, E Lugscheider, Ed., June 2-4, 2008 (Maastricht, The Netherlands), DVS-German Welding Society, 2008.

C. Giolli, G. Rizzi, and **A. Scrivani**, Turbocoating S.p.A., Via Mistrali 7, 43040 Rubbiano di Solignano, Parma, Italy; and **M. Turbil** and **M. Rosso**, Dipartimento di Scienza dei Materiali e Ingegneria Chimica, Politecnico di Torino, Corso Duca degli Abruzzi 24, 10129 Torino, Italy. Contact e-mail: michele.turbil@gmail.com.

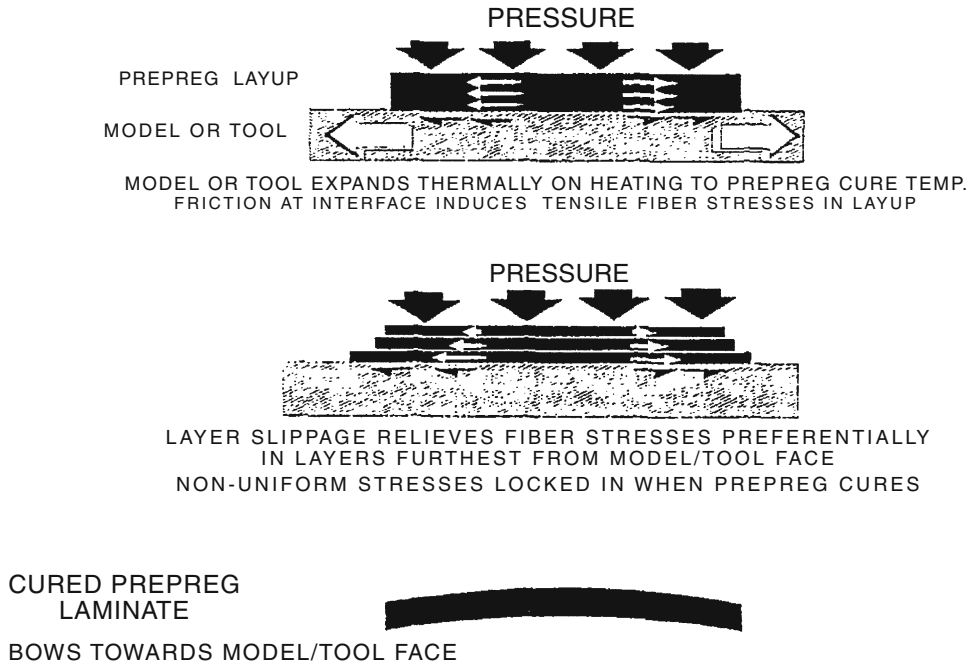

Fig. 1 Interaction between composite laminate and mold during autoclave cure cycle (Ref 6)

the direction from the mold surface, which becomes locked in as the resin cures, so the resultant bending moment warps and detaches from the mold surface the composite component (Fig. 1; Ref 5, 6).

The CTE of a carbon fiber/epoxy component is typically between 2.9 and 3.6 $\times$ 10^{-6}/°C (Ref 7), and the mold materials used for these processes are characterized by low thermal growth properties (i.e., CTE closer than possible to that of the composite component) in the temperature range covered by the curing process (25-177 °C for carbon fiber/epoxy resins), good durability (to ensure high rates of thermal cycling), good surface quality, and vacuum integrity. Several materials have been considered for this application. One is carbon fiber/epoxy resin composite, considered for its low thermal expansion, but it has a short service life because of the surface degradation that results from the thermal cycling processes and rough handling. Even though ceramics and monolithic graphite are good for their thermal growth properties, they are fracture sensitive and difficult to shape. Steel, aluminum, or electroformed nickel are admirable for their durability; however, they have a CTE that is too high (Ref 8). Fe-Ni alloys are characterized by a wide range of CTE values; Fig. 2 shows the variation of the CTE with Ni content and with temperature between −100 and +900 °C for the Fe-Ni binary system. A minimum CTE value of about 1.2 $\times$ 10^{-6}/°C was found for a composition of Fe-35.6%Ni, and it was designated as Invar, meaning invariable. Invar alloy includes workability and durability properties, typical of metallic materials, together with low thermal growth properties, which are typical of ceramic materials (Table 1).

Invar alloy was discovered by the Swiss physicist Charles-Edouard Guillaume in 1896, and for his distinguished work he was awarded the Nobel Prize for Physics in 1920. The Invar alloy has a nominal composition of Fe-36%Ni, is characterized by a completely austenitic structure, and has a very small CTE at room temperature (less than 2 $\times$ 10^{-6}/°C) compared with most metallic materials, which have a CTE of 10 to 20 $\times$ 10^{-6}/°C. Adding the most common alloying elements (Mn, Cr, Ti, Cu, and C) to the Fe-Ni alloy of minimum expansivity can have two effects: one is the variation of the Ni content corresponding to the minimum of the CTE value, and the other is an increase of the minimum, with the exception of Co, which reduces the CTE. Due to the expansion characteristics of the Fe-Ni alloy system, which vary widely depending on composition, more ternary and quaternary low-expansion alloys have been developed to obtain or to intensify secondary properties and/or to increase the ease of fabrication. Invar alloy was initially used in industrial applications that required high dimensional stability, such as precision instruments or liquefied natural gas (LNG) containers, and then for the production of molds for advanced carbon-fiber reinforced plastic (CFRP) components (Ref 9). The main disadvantage of the Invar alloy as mold material is its low coefficient of thermal conductivity (CTC); most common metals have a CTC value included in the range 200-400 W/m K, and the Invar alloy has a CTC value of about 10 W/m K. A mold material with a low CTC value affects the autoclave cure cycles, increasing the heating times of the mold, and which can then cause a decrease in production rates of composite components compared with a mold material with a higher CTC value (Ref 10).

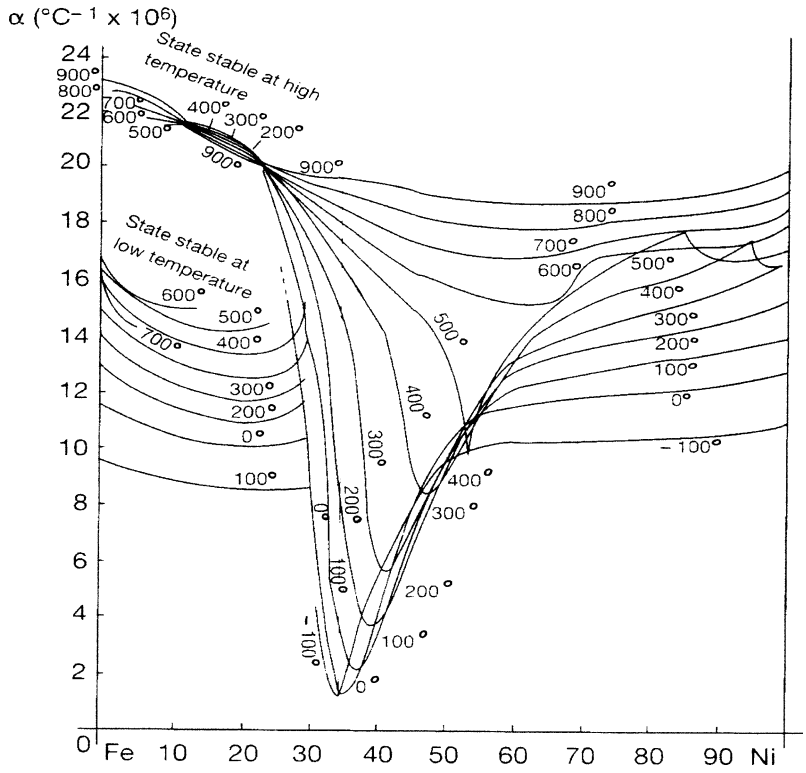

Fig. 2 Variation of Fe-Ni alloys CTE with Ni content and temperature (Ref 9)

Table 1 Mold materials comparison

	Steel, aluminum, electroformed nickel	Graphite/ epoxy resin composite	Ceramics, monolithic graphite	Invar
Low CTE		X	X	X
Durability	X		X	X
Ease of shape forming	X	X		X
Toughness	X	X		X

The main aspects concerning the mold materials for CFRP components can be summarized by: thermal expansion, thermal conductivity, long-term dimensional stability, ease of shape forming, toughness, mold surface quality (as it affects surface quality of resultant composite part), and mold durability.

This work has focused on small-dimension Invar massive molds for automotive components manufacture and on the durability enhancement of the molds using thermal spray coatings.

The critical aspects that had to be considered were:

- Good matching between the CTE of the applied coatings and that of the composite part in order to avoid spring-in and warpage
- Good matching between the CTE of the applied coatings and that of the Invar substrate in order to avoid adhesion problems
- Low mold surface roughness in order to avoid superficial defects in the cured composite part

The aim of this work was to specify through the study of the mechanical and tribological behavior a widely used and well-known thermal spray hard coating with good fracture toughness characteristics that can improve mold durability.

2. Experimental Procedure

2.1 Materials for Coating Deposition

Two series of parallelepiped Invar alloy samples with different dimensions were prepared as substrates to be coated: S1 series (10 mm × 15 mm × 35 mm) for the characterization of the in-section properties of the coatings (microstructural observation, microhardness, and fracture toughness) and S2 series (30 mm × 30 mm × 10 mm) for the characterization of the superficial properties of the coatings (superficial hardness, roughness, friction, and wear testing).

The surface preparation of the Invar samples was done by corundum blasting leading to a substrate roughness of Ra = 9 to 14 μm and by depositing Ni-base and Co-base bond coat layers. Subsequently, the samples were coated with three different kinds of ceramic coatings and with a WC-based cermet coating (top coats).

The ceramic top coats were obtained by spraying commercial ZrO_2-8%Y_2O_3 (−90 + 45 μm), Cr_2O_3 (−15 + 5 μm), and Al_2O_3-13%TiO_2 (−53 + 15 μm) powders using an air plasma spray (APS) process, and the cermet top coat was obtained spraying commercial WC-10%Co-4%Cr (−53 + 11 μm, agglomerated and sintered) powder by means of high-velocity oxygen fuel (HVOF) spray process. The bond coat of the WC-based cermet samples was obtained with the HVOF process, using commercial CoNiCrAlY (−37 + 5 μm) powder and depositing a layer with a thickness in the range 50 ± 10 μm. The bond coat of the Al_2O_3-13%TiO_2 and Cr_2O_3 ceramic samples was obtained with the APS process, using commercial CoMoCrSi (−45 + 15 μm) powder. The thicknesses of the bond coats that resulted from the deposition of CoMoCrSi powder were included in the range 30 ± 5 μm for the Al_2O_3-13%TiO_2 top coat and 20 ± 5 μm for the Cr_2O_3 top coat. Finally, the bond coat of the ZrO_2-8%Y_2O_3 ceramic samples was obtained with the APS process, using commercial Ni-5%Al (−90 + 45 μm) powder, depositing a 1.3 mm thick layer.

The materials and the procedures described previously were used for coating both S1 and S2 series Invar samples. The spraying parameters (gas flow, powder feed rate, and spray distance) were optimized for each coating in order to obtain a coating quality as high as possible; information about torches and spraying parameters, used to deposit HVOF and APS coatings, are not disclosed here because of industrial privacy rights.

2.2 Samples Characterization

Two different kinds of metallographic preparations were used to show the microstructure of the composite HVOF and ceramic APS coatings according to the literature (Ref 11). The thickness and microstructure of the S1 series coated samples were evaluated by SEM analysis (LEO 1450 VP Scanning Electron Microscope, Carl-Zeiss Electron Microscopy Group, Jena, Germany) and porosity by optical microscopy observations (Leica MF-4 optical microscope, Leica Microsystems, Wetzlar, Germany, with Leica QWin v.2 software). The test method B described in the standard ASTM E 2109-01 (Ref 12) was followed for determining the porosity of the coatings: for each coating at least 20 separate fields with 100× of magnification were analyzed.

Vickers microhardness (HV_{100}) of the S1 series coated samples was evaluated by looking at the cross sections under a 100 g normal load applied for 15 s by means of a Leica VMHT Vickers indenter (Leica Microsystems, Wetzlar, Germany). The results are the average values of 30 measurements performed at the bottom, middle, and top of the coatings in five different areas of the cross sections.

Through-thickness fracture toughness (K_{IC}) was obtained by microindentation technique and by applying the Evans-Wilshaw model (Ref 13). Microhardness indentations for calculating K_{IC} were performed at the bottom, middle, and top of the S1 series coated samples in different areas of the cross section and the K_{IC} average values ($MPa\sqrt{m}$) were obtained.

In order to simplify the complex crack morphology typical of the through-thickness indentation (Ref 14), minimum fracture loads necessary to propagate cracks were applied; the average length from the center of indentation to crack ends for each imprint was taken as the c (μm) value (Ref 15, 16) in the Evans-Wilshaw equation, presented in the form:

$$K_{IC} = 0.079 \frac{L}{a^{3/2}} \log \frac{4.5a}{c}$$

where L (mN) is the load applied during the microindentation and a (μm) is the half diagonal length of the imprint.

For a clearer specification of the hardness of the coatings and of the Invar substrate, Rockwell superficial hardness test (R15N) was also carried out on the S2 series coated samples (Ref 17) by means of a Emco-Test hardness tester M4U (Emco-Test, Kuchl, Austria). The S2 series top coats had a thickness in the range 350 to 400 μm in order to avoid substrate influence on hardness measurements according to standard ASTM E 18-05 (Ref 18), and these were ground with diamond disks prior to performing the hardness test in order to minimize the roughness and facilitate measurements. The hardness values were obtained from the average of 10 indentations for each sample.

2.3 Roughness and Wear Testing

The S2 series ceramic coatings used for friction and wear testing were ground with water-lubricated diamond disks and polished with 6 and 1 μm polycrystalline diamond paste to reach a uniform surface roughness of less than 0.8 μm Ra, according to standard ASTM G 99-95a (Ref 19). The cermet coating was ground only with diamond disks to avoid a surface roughness too low in comparison with the ceramic coatings.

The coating roughness was analyzed before and after polishing by a Hommel Tester T1000 stylus profilometer (Hommelwerke, Villingen-Schwenningen, Germany) applying a cut-off value of 0.8 mm and a measurement length of 4.8 mm; three different paths (two perpendicular and one 45° oriented) were covered, and three measurements for each path were performed.

The tribological behavior of the Invar substrate and the S2 series coated samples was investigated in terms of friction coefficient and mass loss using a pin-on-disk configuration in dry sliding conditions and at actual operating temperature (room temperature). The tribometer used for this test was assembled by Polytechnic of Turin in the Alessandria Campus, and it is shown in Fig. 3. The pin used as counterpart had a radiused tip with a radius of 1.5 mm and was made of sintered WC-Co cemented carbide with a hardness of 1600 HV.

The samples were inserted into a rotating cylinder attached to a vertical motor shaft, and the pin was inserted in a pin holder and mounted in the machine; the pin position on the sample and then the path diameter was set by acting on a shift device. The cylinder was then started with a unidirectional sliding motion and the load arm released,

pressing the pin against the sample surface with a normal load. Each test was performed under a 10 N load, with a velocity rotation of 6π rad/s, on a circular path of 24 mm diameter and for 2212 s. The rotating cylinder was cleaned with acetone after each test. The debris were not blown away from the wear track during the friction test, and a new pin was used after each test to ensure identical initial surface conditions.

The coefficient of friction of the Invar substrate and the studied coatings was measured for the total sliding distance of 500 m by recording, with a gap sensor, the displacements of the pin, and the mass loss (10^{-3} g) was measured by weighing the samples before and after the wear tests.

3. Experimental Results and Discussion

3.1 Microstructural and Mechanical Characterization

Different thicknesses and top/bond coat materials were used to meet as closely as possible the following requirements: (1) strengthen the mold surface during the autoclave process, (2) because hard coatings sprayed on a soft substrate are prone to cracking during possible impact loading (Ref 20) and because of the considerable gap in mechanical properties between top coat materials and Invar substrate (Ref 21), allow a gradual decrease of hardness in the direction from the top coat to the substrate to avoid possible damage to the coatings occurring with a rough handling of the mold, (3) accommodate differences between the CTE of the top coat materials and the low CTE of the Invar alloy (Ref 22).

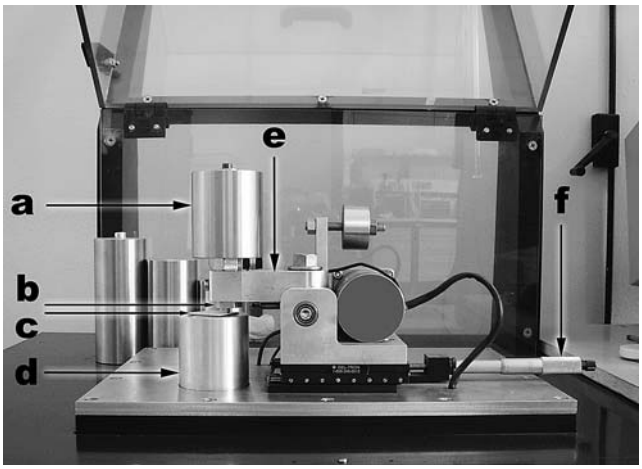

Fig. 3 Pin-on-disk tribometer used for friction and wear testing. (a) 10 N normal load. (b) Pin holder. (c) Sample. (d) Rotating cylinder. (e) Load arm. (f) Shift device

During the solidification of the Invar alloy, the formation of small porosities (2-5 mm) on the mold surface can occur, and some large cavities (10-15 mm) can be hidden just under the mold surface. This phenomenon is caused by the relatively high gap between the density of the solid Invar alloy just under the melting region and the density of the liquid Invar alloy just above the melting region (Ref 23). After several autoclave thermal cycles, the layer of Invar that separates the hidden cavity from the outside can be broken if it is too thin because of the autoclave pressure acting perpendicularly to the mold surface, and the cavity, or a part of it, will appear on the surface. In order to cover the small cavities but mainly to increase the mechanical strength of possible thin layers of Invar that separate a hidden cavity from the outside, Al_2O_3-13%TiO_2 and Cr_2O_3 ceramic materials, which are brittle, were sprayed with a top coat thicker than that of the cermet material, and ZrO_2-8%Y_2O_3, which is brittle and more porous, was deposited with a thin layer on a thick and tough Ni-base bond coat layer, although it does not allow a perfect CTE compatibility between the top coat and the Invar substrate: the measured top coat thicknesses and the CTE values of the coatings and Invar substrate found in the literature (Ref 24-26) are reported in Table 2.

Scanning electron microscopic images showing the thicknesses of the bond and top coats and displaying the coatings microstructure are presented in Fig. 4-6 for the ceramic coatings (ZrO_2-8%Y_2O_3, Al_2O_3-13%TiO_2 and Cr_2O_3, respectively) and in Fig. 7 for the cermet coating.

In the Al_2O_3-13%TiO_2 and Cr_2O_3 coatings, elongated splats form a curved lamellar structure, which is typical for spray formed layers: this structure occurs from the successive deposition of the individual droplets and depends on the spreading and interaction of the splats. Optical and SEM observations pointed out that the Al_2O_3-13%TiO_2 coating contains a low degree of porosity (4-5%) with cracklike flaws and some unmelted and semimelted particles, while in the Cr_2O_3 coating can be seen differences in the porosity distribution between the bottom region of the coating (more dense) and the top region; porosity levels are listed in Table 2. The thin layer lighter in the

Table 2 Selected mechanical and thermal properties of the coatings and the Invar substrate (with standard deviation)

Coating type	Top coat thickness, μm	Porosity level, %	Vickers hardness (sd), HV_{100}	Rockwell hardness (sd), HR_{15N}	Coefficient of thermal expansion, 10^{-6}/°C
Invar			157 (2)	60 (1.57)	~1.20
ZrO_2-8Y_2O_3	300	13-15	860 (130)	73.7 (1.22)	7.6-10.5
Al_2O_3-13TiO_2	1200	4-5	1167 (126)	91.4 (0.41)	~7.40
WC-CoCr	230	5-8	1371 (121)	92.2 (0.40)	~4.30
Cr_2O_3	680	3-5	1534 (128)	93.2 (0.25)	7.40

sd, standard deviation

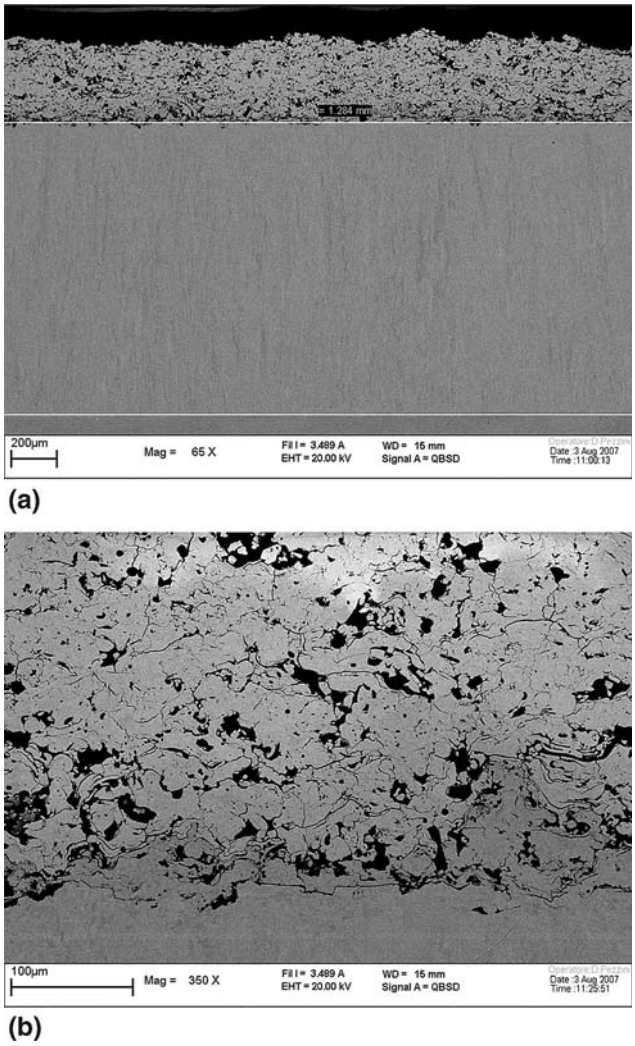

Fig. 4 Scanning electron micrographs of the APS ZrO_2-8%Y_2O_3 coating: (a) thickness; (b) top coat microstructure

Al_2O_3-13%TiO_2 and Cr_2O_3 pictures is the CoMoCrSi bond coat layer: some voids and pinholes were observed in the interface between the Invar substrate and the bond coat, and between the bond coat and the ceramic top coat. In the ZrO_2-8%Y_2O_3 coating was observed the highest degree of porosity among the studied coatings (13-15%). Figure 4(a) shows the thick Ni-Al bond coat applied to the Invar substrate in the case of the ZrO_2-8%Y_2O_3 coating. The WC-CoCr coating is characterized by a finer and thinner splat dispersion if compared with Al_2O_3-13%TiO_2 and Cr_2O_3 coatings and by a relatively low degree of porosity (5-8%).

Furthermore, the CoNiCrAlY alloy used for the bond coat in the cermet coating was replaced by the CoMoCrSi alloy for the bond coat deposition in the case of Al_2O_3-13%TiO_2 and Cr_2O_3 coatings because the amounts of molybdenum (28%) and silicon (2%) in the CoMoCrSi powder are added at levels in excess of their

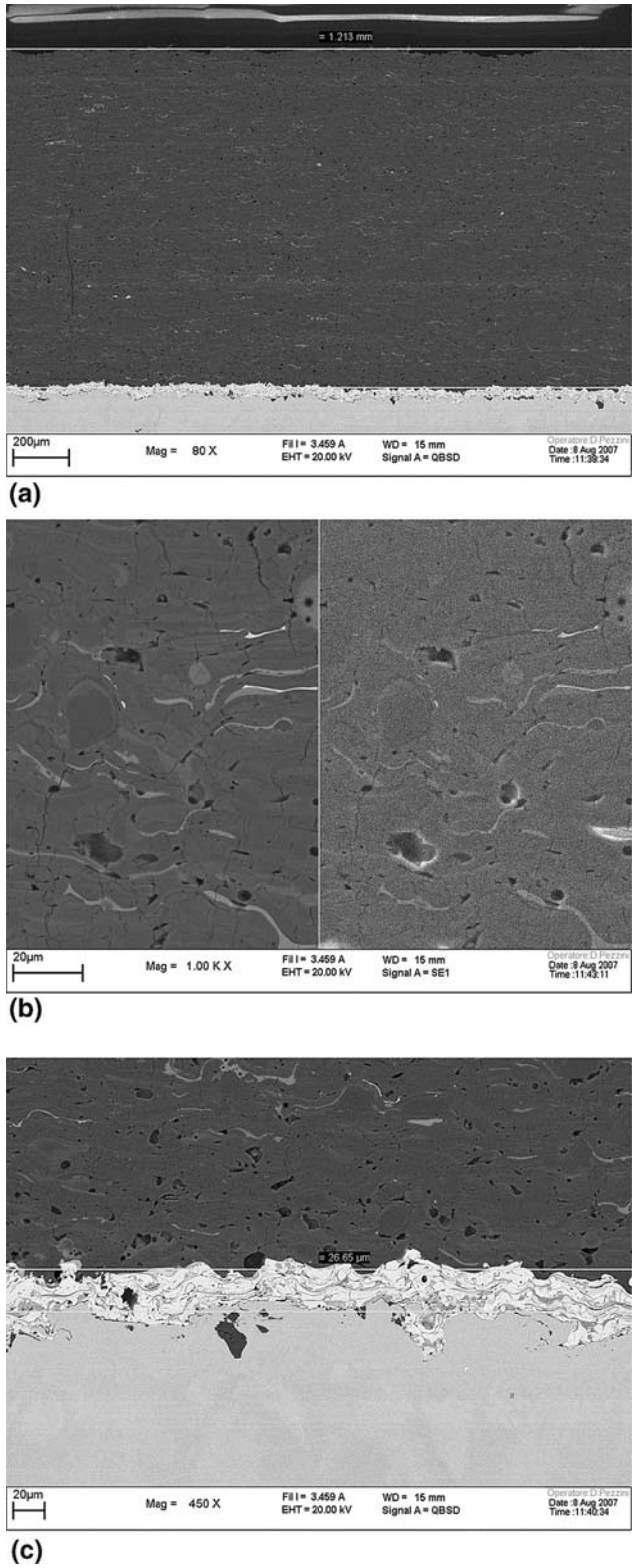

Fig. 5 Scanning electron micrographs of the APS Al_2O_3-13%TiO_2 coating. (a) Thickness. (b) Top coat microstructure in backscattered electrons mode and in secondary electrons mode. (c) Bond coat

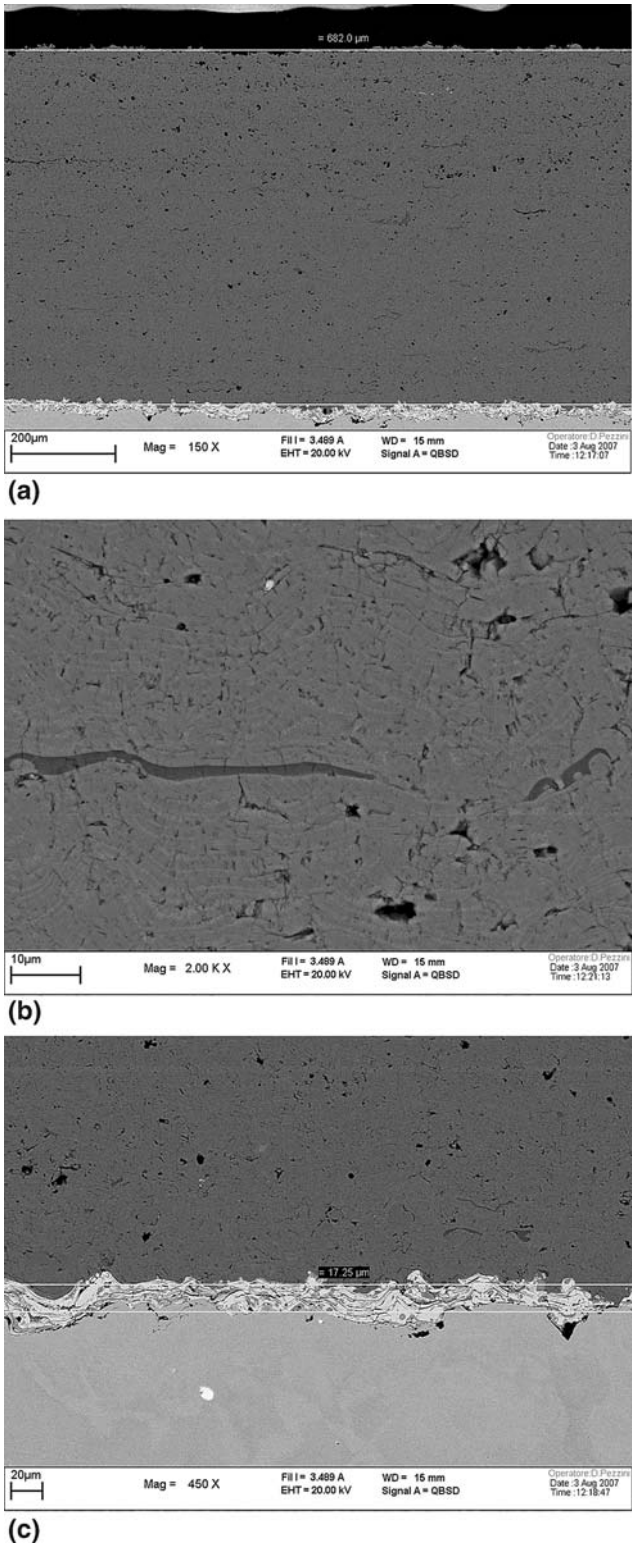

Fig. 6 Scanning electron micrographs of the APS Cr_2O_3 coating. (a) Thickness. (b) Top coat microstructure. (c) Bond coat

solubility limit, inducing the precipitation of the hard Laves phase (CoMoSi or Co_3Mo_2Si; Ref 27) and allowing a more gradual variation of hardness from the hard and brittle top coat to the soft and tough Invar substrate.

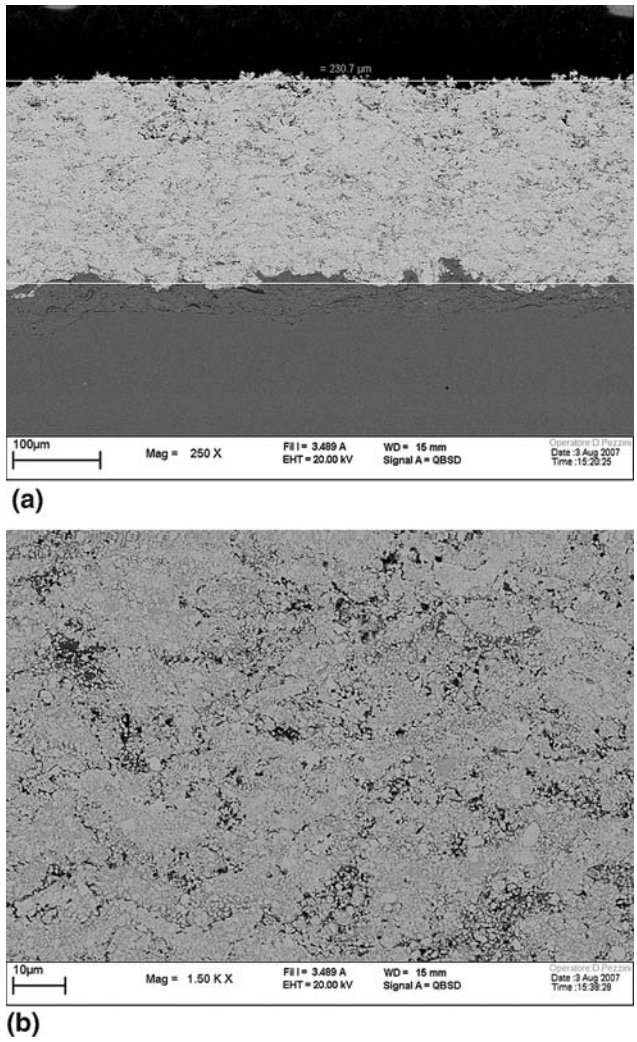

Fig. 7 Scanning electron micrographs of the HVOF cermet coating. (a) Thickness. (b) Top coat microstructure

The average of the microhardness values (HV_{100}) and the average of the superficial Rockwell hardness values (R15N) with standard deviations for the top coatings and the Invar substrate are reported in Table 2. In the Al_2O_3-13%TiO_2, WC-CoCr, and Cr_2O_3 coatings were found higher microhardness values compared with the ZrO_2-8%Y_2O_3 coating, and all the coatings are much harder than Invar substrate, which has very low microhardness and superficial hardness values (157 HV_{100} and 60 HR_{15N}, respectively). The superficial hardness measurements confirm the same order of hardness obtained on the coatings with the in-section microhardness measurements; higher hardness values ensure a better wear behavior of the coated Invar mold.

Through-thickness fracture toughness average values, minimum loads applied for each coating, and parameters used for the evaluation of the fracture toughness by the

Table 3 Parameters used in the Evans-Wilshaw equation and through-thickness fracture toughness values (with standard deviation) of the S1 series coatings

Coating type	*a*, μm	*c*, μm	*L*, mN	K_{IC} (sd), MPa$\sqrt{m}$
ZrO_2-8Y_2O_3				
Bottom	15	28.0	2940	1.53 (0.04)
Middle	14	27.7		
Top	13	29.0		
Al_2O_3-13TiO_2				
Bottom	11	19.80	2940	2.46 (0.14)
Middle	10	20.00		
Top	9	21.75		
Cr_2O_3				
Bottom	9	14	2940	3.57 (0.30)
Middle	10	15		
Top	10	16		
WC-CoCr				
Bottom	34	39.0	19600	4.44 (0.13)
Middle	33	43.3		
Top	30	46.5		

sd, standard deviation

Evans-Wilshaw equation are listed in Table 3. The *c* values are all included in the validity range for the Evans-Wilshaw equation: $0.6 \leq c/a \leq 4.5$. The highest K_{IC} value was found in the WC-CoCr coating (~4.5 MPa$\sqrt{m}$), and the highest K_{IC} value among the ceramic coatings was obtained with Cr_2O_3 (~3.6 MPa$\sqrt{m}$), while the Al_2O_3-13%TiO_2 and ZrO_2-8%Y_2O_3 coatings showed lower K_{IC} values, respectively, about 2.5 and 1.5 MPa$\sqrt{m}$. Low standard deviation values denote a constant behavior of the fracture toughness all through the thickness of the coatings, and higher fracture toughness values prevent crack formation on the surface of the coated Invar mold caused by possible impact loading.

3.2 Roughness

Mold surface porosities/cavities and roughness can affect the surface quality of the cured composite part, no matter the material of the mold. The relatively large porosities and cavities on the surface of the bare Invar mold can permit in-flow of still not cured resin and generate a mechanical clamping that locks to the mold the first laminate of the composite component and makes difficult the removal of the component after curing process. Mold surface roughness causes a poor adherence of the part to the mold, and the composite component after cure will not be within the tight dimensional tolerances required. Furthermore, both mold surface porosity and roughness cause a rough composite part surface. Several release agents can be used to help remove the part from the mold (Ref 1, 2, 4), but they cannot compensate for a lack in mold surface preparation; thus, minimizing the coating roughness is a key factor in obtaining a composite component that takes the exact mirror image of the mold.

The high porosity and relatively low cohesion of the ZrO_2-8%Y_2O_3 coating did not allow the decrease in surface roughness below a minimum obtainable value (1.2 μm), while the lamellar structure of the Al_2O_3-13%TiO_2 and Cr_2O_3 coatings jointly with their higher hardness values allowed to reach a surface roughness of 0.3 μm. Although Invar and WC-CoCr coatings could have been polished down to a lower roughness value with buffing, finishing operations were stopped at 0.1-0.2 μm to avoid an excessive gap with the ceramic coatings and to make friction and wear test results comparable. The highest roughness reduction during the finishing operations was obtained with the ZrO_2-8%Y_2O_3 coating (from 8.9 to 1.2 μm), and the lowest was obtained with the Cr_2O_3 coating (from 3.4 to 0.3 μm). The lowest roughness value was obtained with the WC-CoCr cermet coating; roughness average values of the S2 series coatings before and after polishing with standard deviations are listed in Table 4.

Table 4 Surface roughness of the as coated and polished S2 samples (with standard deviation)

Coating type	As-coated S2 samples Ra (sd), μm	Polished S2 samples Ra (sd), μm
Invar		0.16 (0.04)
ZrO_2-8Y_2O_3	8.9 (0.62)	1.20 (0.10)
Al_2O_3-13TiO_2	4.9 (0.36)	0.26 (0.02)
Cr_2O_3	3.4 (0.16)	0.30 (0.02)
WC-CoCr	3.7 (0.17)	0.10 (0.01)

sd, standard deviation

During grinding operations Al_2O_3-13%TiO_2 and Cr_2O_3 plasma sprayed coatings showed a different behavior from HVOF cermet coating; when the top surface of the Al_2O_3-13%TiO_2 and Cr_2O_3 coatings was pressed against the abrasive disk with a normal load, the lamellar structure of the coatings was parallel to the motion direction of the disk and opposed a weak resistance to the shear stresses generated from the disk motion, probably because of a low interlamellar cohesion. This behavior allowed progressive removal of the superficial splats of the coatings with a relatively low normal load, although the hardness of the coatings was high (Cr_2O_3 showed the highest hardness value among the studied coatings). The finer and thinner splat structure of the cermet coating showed a higher resistance to the action of the disk, and it was necessary to apply a higher load and take much more time to reach about the same roughness values of the Cr_2O_3 coating, although the cermet coating had a hardness value lower than that of the Cr_2O_3 coating.

3.3 Friction and Wear Testing

The autoclave environment in which the curing process develops is neither an oxidative nor a corrosive environment, and the temperature at which the epoxy resins cure (177 °C) is very low if compared with the higher temperatures that the examined coatings are able to tolerate. Then, considering the low hardness value of Invar alloy and that the wear action occurs at room temperature, each sprayed coating can significantly improve the wear resistance of the mold and extend its working life compared

Table 5 Average coefficients of friction and mass losses of the Invar substrate and the sprayed coatings for a sliding distance of 500 m (with standard deviation)

Coating type	Average friction coefficient 0-500 m (sd)	Mass loss, 10^{-3} g (sd)
Invar	0.63 (0.15)	8.8 (3.90)
ZrO_2-8Y_2O_3	0.81 (0.10)	2.8 (0.83)
Al_2O_3-13TiO_2	0.86 (0.08)	0.8 (0.14)
Cr_2O_3	0.64 (0.12)	1.0 (0.15)
WC-CoCr	0.57 (0.07)	0.7 (0.07)

sd, standard deviation

with the bare Invar mold. The friction and wear tests were carried out to realize a comparative study among the sprayed coatings that specify the coating with the best wear behavior.

The average coefficients of friction and mass losses with standard deviations obtained in the tribological tests are listed in Table 5. Among APS sprayed ceramic coatings, Cr_2O_3 had the lowest average friction coefficient and Al_2O_3-13%TiO_2 exhibited the best wear behavior. The WC-CoCr cermet coating had the lowest average friction coefficient and showed the best wear behavior among all the studied coatings. Furthermore, the highest mass loss among the coatings was verified with the ZrO_2-8%Y_2O_3 coating; Al_2O_3-13%TiO_2, Cr_2O_3, and WC-CoCr coatings revealed better wear behavior compared with the ZrO_2-8%Y_2O_3 coating and the Invar substrate.

The friction coefficient value of the Invar substrate measured during the tribological test was affected by the stick-slip behavior (Ref 28). The low hardness and high ductility of the Invar alloy determined the formation of strong junctions between the pin and the sample and induced the increase of the friction coefficient. Under the action of the sliding force, applied from the tribosystem, the junctions were broken and the sliding speed between the pin and the sample raised suddenly. During this step, new but much less strong junctions were formed, inducing the decrease of the friction coefficient. Then the sliding speed returned to the constant value applied from the tribosystem, inducing the formation of new strong junctions.

Stick-slip behavior determined a wide range of excursion for the friction coefficient (Fig. 8a), explaining the relatively low friction coefficient average value of the Invar substrate compared with its high mass loss and compared with the friction coefficient average values of the sprayed coatings. Figure 9 shows the scanning electron micrograph of the wear track on the Invar substrate: the high ductility of Invar alloy determined a high deformation of the sample during the friction test. Because of the slick-slip behavior the wear track assumed a ''sea waves-like'' morphology that was formed just after the initial stages of the friction test and then the pin, hitting against the wave crests, wore away high amounts of metal from the Invar sample. It was observed that stick-slip behavior, which was verified for the Invar alloy also in a tribological test performed with a 5 N load and which is easily recognizable because the tribosystems that display this behavior often produce vibrations and noise (Ref 28), did not occur with the coatings.

The frictional and wear behavior of the ZrO_2-8%Y_2O_3 ceramic APS sprayed coating was affected by the high roughness and porosity values and by the low hardness that determined a high mass loss compared with the other studied coatings. The morphological and mechanical characteristics of the ZrO_2-8%Y_2O_3 coating induced an abrasive wear behavior during the development of the tribological test. The detection of amounts of W, C, and Co in the wear track performed by EDS semiquantitative investigations revealed the formation in the wear track of a thin and soft surface film consisting of ZrO_2-8%Y_2O_3 wear debris and material transferred from the pin to the sample. Then the last stages of the friction test were probably performed on the soft film formed during the initial stages and not on pure ZrO_2-8%Y_2O_3, generating a higher friction coefficient and a probably lower mass loss in comparison with the initial stages of the test. An example of the evolution of friction coefficient obtained during the tribological test for ZrO_2-8%Y_2O_3 coating is displayed in Fig. 8(b): after a rapid rise during a short initial stage of the test, the friction coefficient oscillated approximately around the same value for a wide range of the sliding distance and then started again to increase slowly before the end of the test because of the gradual formation of the tribofilm. Figure 10 shows the scanning electron micrograph of the wear track on the ZrO_2-8%Y_2O_3 coating in backscattered electrons mode (left) and in secondary electrons mode (right), and the differences between the smooth surface of the polished ZrO_2-8%Y_2O_3 sample (extreme right of the micrograph) and the irregular and excavated morphology of the wear track are pointed out.

Both Al_2O_3-13%TiO_2 and Cr_2O_3 ceramic APS sprayed coatings exhibited an adhesive wear behavior because of the lower porosity levels and because of the higher hardness values if compared with those of the ZrO_2-8%Y_2O_3 APS coating, and then lower mass losses were obtained. Touching asperities of the sample and the counterpart adhered together because of the applied load, and the tips of the less hard material were ''plucked'' off, adhering to the surface of the harder material (Ref 29). The Cr_2O_3 coating exhibited an average friction coefficient lower and a mass loss higher than that of the Al_2O_3-13%TiO_2 coating; this behavior is probably caused by the transfer and adhesion to the Cr_2O_3 coated sample surface of a little amount of pin material that formed during the friction test a thin and smooth tribofilm affecting the friction coefficient value. The presence of the tribofilm was revealed by EDS semiquantitative investigations. The left side of Fig. 11, showing the scanning electron micrograph of the wear track on the Al_2O_3-13%TiO_2 coating in backscattered electrons mode, points out that elements others than those forming the coating are not present and also that the tribofilm was not formed in the Al_2O_3-13%TiO_2 coating wear track. The tribofilm formed on the surface of the Cr_2O_3 coated sample is shown in Fig. 12 (scanning electron micrograph of the wear track on the Cr_2O_3 coating in

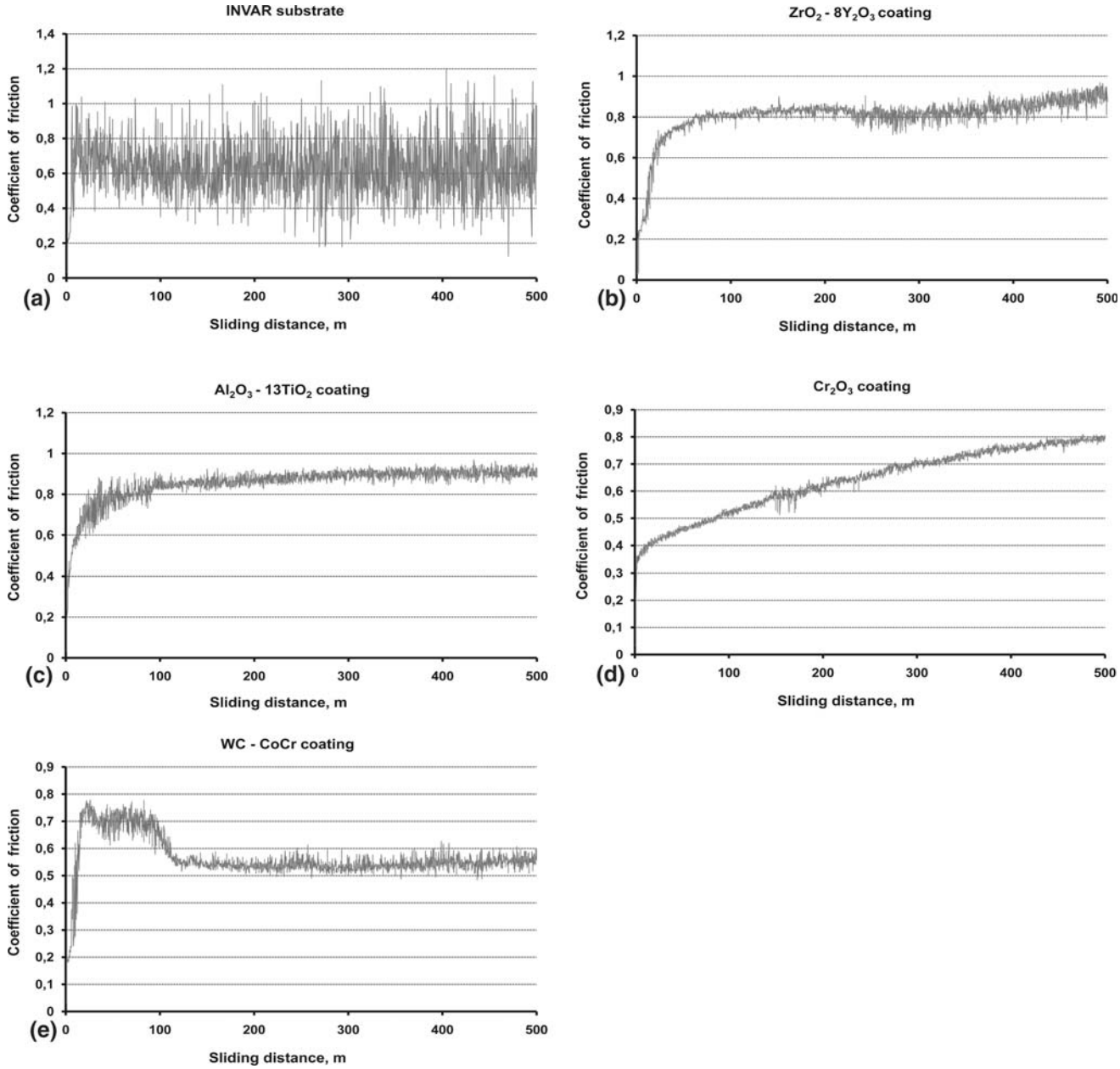

Fig. 8 Friction coefficients evolution obtained during the total sliding distance of the tribological tests for the Invar substrate and the sprayed coatings. (a) Invar. (b) ZrO_2-8%Y_2O_3. (c) Al_2O_3-13%TiO_2. (d) Cr_2O_3. (e) WC-CoCr

backscattered electrons mode and in secondary electrons mode). During the Cr_2O_3 friction test, a part of the tribofilm was detached from one side of the wear track, giving rise to wear particles or fragments and determining a higher mass loss compared with the Al_2O_3-13%TiO_2 coating, in spite of the higher hardness value of the Cr_2O_3 coating. The influence of the tribofilm on the coefficient of friction of the Cr_2O_3 coating was also revealed by comparing the evolution of the friction coefficients for the Al_2O_3-13%TiO_2 and the Cr_2O_3 coatings. An example of the evolution of the friction coefficient obtained during the tribological test for both Al_2O_3-13%TiO_2 and Cr_2O_3 coatings is displayed in Fig. 8(c) and (d), respectively. The Cr_2O_3 coating friction coefficient increased slowly for the duration of the tribological test, maintaining its value relatively low for the most of the sliding distance, and then also its average value, referred to the total sliding distance, stayed relatively low. In contrast, Al_2O_3-13%TiO_2 friction coefficient rose immediately, maintaining a higher value than that of the Cr_2O_3 coating for the most of the sliding distance, and then also its average value, referred to the total sliding distance, rose higher than that obtained with the Cr_2O_3 coating. The progressive increase of the friction coefficient of the Cr_2O_3 coating is caused by the amount of

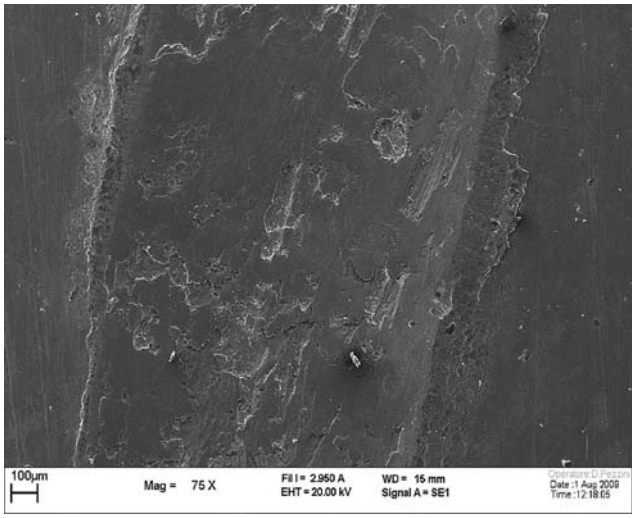

Fig. 9 Scanning electron micrograph of the wear track formed on the Invar substrate

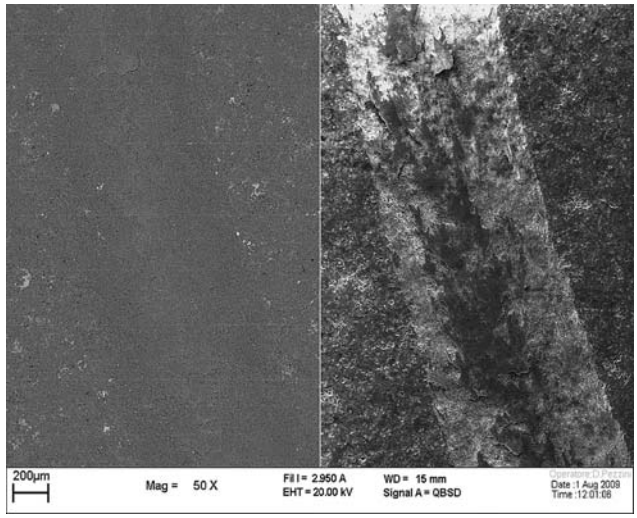

Fig. 11 Scanning electron micrograph of the wear track formed on the Al_2O_3-13%TiO_2 coating in backscattered electrons mode (*left*) and in secondary electrons mode (*right*)

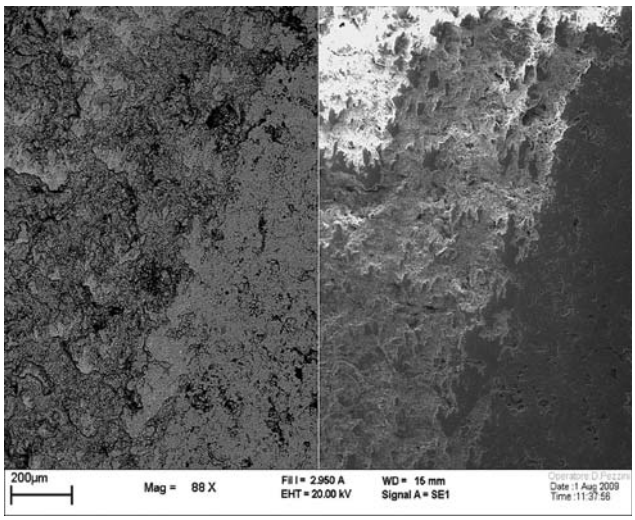

Fig. 10 Scanning electron micrograph of the wear track formed on the ZrO_2-8%Y_2O_3 coating in backscattered electrons mode (*left*) and in secondary electrons mode (*right*)

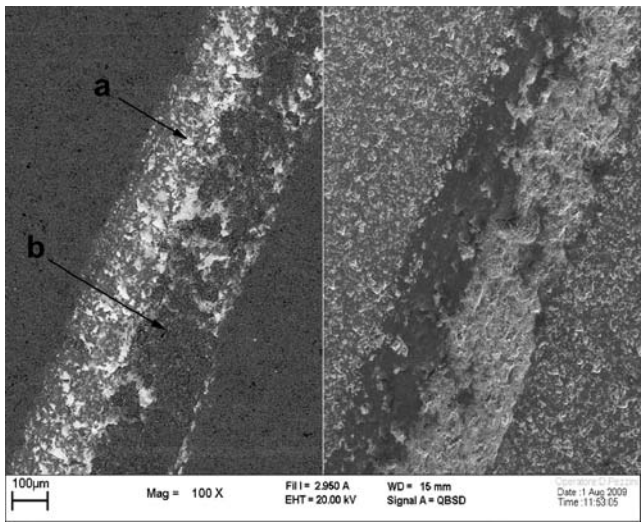

Fig. 12 Scanning electron micrograph of the wear track formed on the Cr_2O_3 coating in backscattered electrons mode (*left*) and in secondary electrons mode (*right*) showing the tribofilm (a) and the side of the wear track from which the tribofilm was detached (b)

pin material transferred to the sample surface: during the friction test, many touching asperities went from an interaction Cr_2O_3/pin material to an interaction pin material/pin material, and because this second kind of interaction is characterized by a higher work of adhesion the coefficient of friction increased.

The WC-CoCr coating had the lowest friction coefficient average value and the lowest mass loss among all the studied coatings: these results are probably caused by the high hardness and the very low roughness value reached after polishing operations, besides the finer and thinner splat dispersion typical of the WC-CoCr morphological structure in opposition to the lamellar structure of the Al_2O_3-13%TiO_2 and Cr_2O_3 coatings. Furthermore, the WC-CoCr coating exhibited an oxidation-dominated wear behavior with the formation, during the friction test, of a thin and discontinuous oxide layer on the surface of the sample, which performed a lubricating and protective action. The oxide layer was revealed by EDS semiquantitative investigations. Figure 13 (scanning electron micrograph of the wear track on the WC-CoCr coating in backscattered electrons mode, left, and in secondary electrons mode, right) shows the areas of the wear track in which the oxide layer was formed, and Fig. 14 shows the cracks in the oxide layer that occurred during the test. The influence of the oxide layer on the evolution of the coefficient of friction of the WC-CoCr coating is shown in Fig. 8(e); after a rapid rise during a short initial stage of

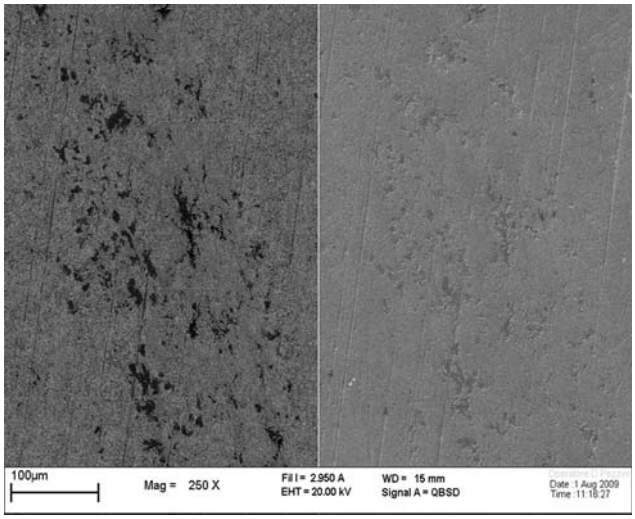

Fig. 13 Scanning electron micrograph of the wear track formed on the WC-CoCr coating in backscattered electrons mode (*left*) and in secondary electrons mode (*right*)

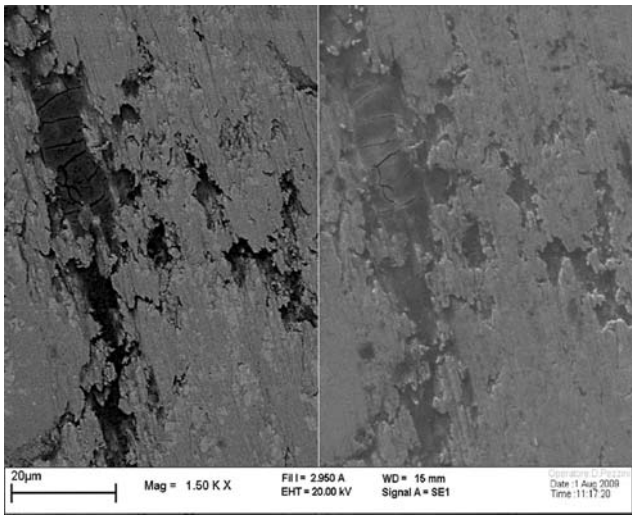

Fig. 14 Scanning electron micrograph of the oxide layer cracks formed in the WC-CoCr coating wear track in backscattered electrons mode (*left*) and in secondary electrons mode (*right*)

the test, the friction coefficient oscillated approximately around the same upper value for a narrow range of the sliding distance and then decreased and started to oscillate around a lower value as a result of the formation of the oxide layer.

4. Conclusions

Molds for the production of CFRP components are typically made of Invar alloy (Fe-36%Ni), which is characterized by a very low hardness value and by a poor wear behavior. Three plasma sprayed ceramic coatings, ZrO_2-8%Y_2O_3, Al_2O_3-13%TiO_2, and Cr_2O_3, and a HVOF cermet coating (WC-10%Co-4%Cr) were characterized in term of mechanical and tribological properties in order to specify a coating that can improve the durability of small-dimension Invar massive molds.

Stating that among the studied coatings the CTE of the HVOF cermet coating better approximated the CTE of the bare Invar mold and then exhibited the best CTE compatibility with the CFRP to be cured, the experimental results lead to the following conclusions:

- Both APS ceramic coatings and HVOF cermet coating enhanced the Invar alloy wear behavior. Al_2O_3-13%TiO_2 APS sprayed coating and HVOF cermet coating improved up to 1 order of magnitude the wear resistance of the Invar alloy.
- Both APS ceramic coatings and HVOF cermet coating enhanced the Invar mold hardness. Furthermore, Cr_2O_3 APS sprayed coating and HVOF cermet coating showed the highest fracture toughness values.
- Among the APS coatings, Al_2O_3-13%TiO_2 reached the lowest roughness level after polycrystalline diamond paste polishing and the HVOF cermet coating reached the lowest roughness level among all the examined coatings, ensuring the best quality of a mold surface.

Acknowledgments

The authors acknowledge Ing. Dario Pezzini and Ing. Enrico Pallavicini from the Alessandria Campus of the Polytechnic of Turin for the technical support and their experience in conducting tests. The authors thank Mr. Gennaro Cirillo of Parma Spray Italia S.p.A. for his help in thermal spray trials and Landra S.p.A. for the Invar alloy.

References

1. N. Ersoy, K. Potter, M.R. Wisnom, and M.J. Clegg, An Experimental Method to Study the Frictional Processes During Composites Manufacturing, *Compos. Part A*, 2005, **36**(11), p 1536-1544
2. G. Fernlund, N. Rahman, R. Courdji, M. Bresslauer, A. Poursartip, K. Willden, and K. Nelson, Experimental and Numerical Study of the Effect of Cure Cycle, Tool Surface, Geometry, and Lay-Up on the Dimensional Fidelity of Autoclave-Processed Composite Parts, *Compos. Part A*, 2002, **33**(3), p 341-351
3. D.W. Radford and T. Rennick, Separating Sources of Manufacturing Distortion in Laminated Composites, *J. Reinf. Plast. Compos.*, 2000, **19**(8), p 621-641
4. C. Albert and G. Fernlund, Spring-in and Warpage of Angled Composite Laminates, *Compos. Sci. Technol.*, 2002, **62**(14), p 1895-1912
5. K.D. Potter, M. Campbell, C. Langer, and M.R. Wisnom, The Generation of Geometrical Deformations due to Tool/Part Interaction in the Manufacture of Composite Components, *Compos. Part A*, 2005, **36**(2), p 301-308
6. C. Ridgard, Accuracy and Distortion of Composite Parts and Tools: Causes and Solutions, *Tooling for Composites '93,* 18-19 Jan 1993 (Pasadena, CA), Society of Manufacturing Engineers, 1993, EM93/113, p 1-18

7. S.L. Abberger, Advanced Composite Molds—A New Use for Invar, *The Invar Effect: A Centennial Symposium*, J. Wittenauer, Ed., 7-8 Oct 1996 (Cincinnati, OH), The Minerals, Metals & Materials Society, 1997, p 317-325
8. W.R. Schell, Invar Tooling for Composites, *Tooling for Composites '89,* 21 June 1989 (Long Beach, CA), Society of Manufacturing Engineers, 1989, TE89/503, p 1-13
9. F. Duffaut and R. Cozar, Property Adjustments in Controlled Expansion and Elasticity Alloys, *The Iron-Nickel Alloys. A Hundred Years after the Discovery of Invar*, G. Béranger et al., Ed., Lavoisier Publishing, 1996, p 109-139
10. Appendix, *The Invar Effect: A Centennial Symposium,* J. Wittenauer, Ed., Oct 7-8 1996 (Cincinnati, OH), The Minerals, Metals & Materials Society, 1997, p 339
11. W. Riggs, K. Couch, and K. Larson, Metallography and Image Analysis, *Handbook of Thermal Spray Technology*, J.R. Davis, Ed., ASM International, 2005, p 224-259
12. "Test Methods for Determining Area Percentage Porosity in Thermal Sprayed Coatings," E 2109-01, *Annual Book of ASTM Standards*, Part 03.01, ASTM International, p 1228-1235
13. A.G. Evans and T.R. Wilshaw, Quasi-Static Solid Particle Damage in Brittle Solids—I. Observations, Analysis and Implications, *Acta Metall.*, 1976, **24**(10), p 939-956
14. E. Lopez Cantera and B.G. Mellor, Fracture Toughness and Crack Morphologies in Eroded WC-Co-Cr Thermally Sprayed Coatings, *Mater. Lett.*, 1998, **37**(4-5), p 201-210
15. C.B. Ponton and R.D. Rawlings, Vickers Indentation Fracture Toughness Test. Part 1: Review of Literature and Formulation of Standardised Indentation Toughness Equations, *Mater. Sci. Technol.*, 1989, **5**, p 865-872
16. C.B. Ponton and R.D. Rawlings, Vickers Indentation Fracture Toughness Test. Part 2: Application and Critical Evaluation of Standardised Indentation Toughness Equations, *Mater. Sci. Technol.*, 1989, **5**, p 961-976
17. W. Riggs and K. Couch, Testing of Coatings, *Handbook of Thermal Spray Technology*, J.R. Davis, Ed., ASM International, 2005, p 260-261
18. "Standard Test Method for Rockwell Hardness and Rockwell Superficial Hardness of Metallic Materials," E 18-05, *Annual Book of ASTM Standards,* Part 03.01, ASTM International, p 130-151
19. "Standard Test Method for Wear Testing with a Pin-on-Disk Apparatus," G 99-95a (Reapproved 2000), *Annual Book of ASTM Standards,* Part 03.02, ASTM International, p 414-419
20. C. Pfohl and K.T. Rie, Plasma Duplex Treatment of Stellite, *Surf. Coat. Technol.*, 2001, **142-144**, p 1116-1120
21. Appendix, *The Invar Effect: A Centennial Symposium,* J. Wittenauer, Ed., 7-8 Oct 1996 (Cincinnati, OH), The Minerals, Metals & Materials Society, 1997, p 339-346
22. F.N. Longo, Coating Processing, *Handbook of Thermal Spray Technology*, J.R. Davis, Ed., ASM International, 2005, p 115-116
23. A. Seifter, K. Boboridis, B. Didoukh, G. Pottlacher, and H. Jäger, Thermophysical Properties of Liquid Fe64/Ni36 (INVAR), *J. Chim. Phys.*, 1997, **94**, p 1004-1008
24. R.L. Lehman, Overview of Ceramic Design and Process Engineering, *Ceramics and Glasses,* Vol 4, *Engineered Materials Handbook,* ASM International, 1991, p 30
25. P.T.B. Shaffer, Engineering Properties of Carbides, *Ceramics and Glasses,* Vol 4, *Engineered Materials Handbook,* ASM International, 1991, p 809
26. R. Kamo, Adiabatic Diesel Engines, *Ceramics and Glasses,* Vol 4, *Engineered Materials Handbook,* ASM International, 1991, p 990
27. Selected Applications, *Handbook of Thermal Spray Technology,* J.R. Davis, Ed., ASM International, 2005, p 177
28. "Standard Guide for Measuring and Reporting Friction Coefficients," G 115-98, *Annual Book of ASTM Standards,* Part 03.02, ASTM, p 499-509
29. J. Williams, *Engineering Tribology*, Cambridge University Press, 2005, p 176